Spatially resolved and energy-resolved defect kinetics in *a*-Si:H: A comprehensive study by phase-shift analysis of modulated photocurrents

G. Schumm and G. H. Bauer
Institut für Physikalische Elektronik, Universität Stuttgart, Pfaffenwaldring 47, D-7000 Stuttgart 80, Federal Republic of Germany
(Received 15 August 1988)

The analysis of modulated photocurrents is reviewed, and a novel experimental technique for measurements of modulated photocurrents over a wide frequency range is applied to undoped *a*-Si:H in sandwich contact configuration. By analysis of the phase response the energetic as well as spatial (versus distance to the top contact) distribution of gap states above midgap is obtained. Metastable changes in the gap-state distribution by light soaking (Staebler-Wronski effect) and by depletion bias annealing are studied as a function of illumination time, illumination temperature, annealing time, annealing temperature, and applied bias during annealing. The main experimental results are as follows: Undoped *a*-Si:H exhibits a peak in the distribution of gap states at about 0.6 eV below the conduction-band edge E_c and in the depletion region a peak of shallow states at 0.4 eV below E_c. Upon light soaking the deep peak increases according to a power law and the shallow one is quenched. The original distribution is restored by annealing above 420 K. At lower degradation temperatures, creation and quenching rates are enhanced but the established changes are less stable against annealing. Both peaks show exponential tails towards midgap with slopes that depend on annealing and degradation temperatures. Activation energies for annealing of deep states show a broad variation between 0.9 and 1.3 eV and are strongly correlated with the energetic position of the defect states in the gap. Annealing with depletion bias produces a metastable increase of both defect peaks above midgap. Based on the thermodynamical considerations and on theoretical calculations of the dangling-bond correlation energies, a model of the defect structure is discussed that is able to account for the presented results as well as various other experimental observations concerning metastable changes and the energetic position of defects in amorphous silicon.

I. INTRODUCTION

The negatively charged dangling-bond (D^-) states in *a*-Si:H have been located at two different energetic positions in the gap, either at about 0.6 eV or at about 0.9 eV below the conduction-band edge E_c, depending on the experimental technique that has been used. A summary of reported results and references thereof has been given by LeComber and Spear.[1] There have been several attempts to explain this discrepancy: One reason might be that the different levels refer to the isolated D^- at 0.6 eV and to a charge-coupled state of the D^- with a P^+ (ionized phosphorous atom) lowering the energy of the D^- by Coulomb interaction to $E_c-0.9$ eV.[2,3] Another model has been introduced by Bar-Yam and co-workers. Based on *ab initio* total-energy calculations they find potential sites for the Si-DB distributed throughout the gap, depending on the distortion of the surrounding network, and small effective correlation energies for different charge occupations.[4] The actual density-of-states (DOS) distribution is established by freeze-in of a thermodynamical equilibrium defect structure when cooling the sample below a transition temperature T^*. For the dangling bonds (DB's) this will result in a peak of D^+ centers above and a peak of D^- centers below the Fermi level E_F during freeze-in and exponential tails towards E_F.[5] Shifting E_F by doping or applied bias will change the DOS accordingly and enhance or quench the D^+ and/or D^- peaks, respectively. Thus, the position and size of the defect peaks is not primarily determined by Coulomb interactions with doping atoms but is due to the actual formation energies of defects that depend in case of charged defects sensitively on the Fermi level.

Recently we have reported on two DOS peaks in undoped *a*-Si:H at ≈ 0.6 eV and ≈ 0.4 eV below E_c determined by means of phase-shift analysis of modulated photocurrents.[6,7] Upon light soaking the shallow peak was quenched and the deep one increased, the original distribution was obtained by annealing above 420 K. In this paper the analysis of modulated photocurrents is reviewed with special emphasis on measurements in sandwich-contact configuration, and the influence of experimental parameters on the results is investigated. We present quantitative results for defect formation and annealing on undoped *a*-Si:H. The defect density is found to obey the $t^{1/3}$ law;[8] activation energies for annealing have been determined; the shape of the defect peaks could be evaluated, they show exponential tails towards the Fermi level; depletion bias annealing resulted in an enhancement of the peaks; from spatial resolution of the DOS (versus distance to the sample-contact interface) it was found that the band bending at a Shottky interface also enhances the deep peak and shifts the peak maximum towards midgap. It is shown that our results are in agreement with the thermodynamical model developed by Bar-Yam and co-workers.

II. PHASE-SHIFT ANALYSIS OF MODULATED PHOTOCURRENTS

A. General description

Photocarriers in an a-Si:H sample are generated band-to-band by sinusoidally modulated light and the resulting photocurrent is measured in terms of amplitude and phase lag with respect to the excitation signal as a function of modulation frequency. Experimental details are given elsewhere.[6,7] Thus, in principle, the physical processes involved are similar to transient experiments, where excess charge carriers are optically generated by a light pulse and their return to equilibrium is monitored as a function of time, namely, transient photocurrent and time-of-flight (TOF) measurements with coplanar and sandwich-contact configurations. But there are some differences.

(1) In transient experiments the energy range for which the DOS can be evaluated is given by the experimentally accessible time window (limited to short times by the response time of the measurement circuit and to long times by the fast decay of transient signals, especially in view of the dark currents involved), yielding tail-state distributions typically from 80 to 200 meV below the transport path of charge carriers.[9] In comparison, measurements of signals in the frequency domain are limited by the bandwidth of the photocurrent amplifier, yielding the gap-state distribution for deep states—from the Fermi level up to about 200 meV below the transport path.

(2) Use of lock-in techniques in the frequency domain with improved signal-to-noise ratios allow by orders of magnitudes smaller excitations and thus lower deviations from dark thermal equilibrium. Possible structural changes by light during the measurements can be kept to a minimum. Possible nonlinearities of the sample response, e.g., electron-electron interactions or trap saturation, are also expected to be smaller.

(3) Dark currents as well as currents due to other effects like field redistribution (dielectric relaxation) are screened out by the lock-in technique provided that they do not have periodical contributions at the modulation frequency.

(4) When measuring in the TOF configuration, the free-carrier transit time is very short compared to the time window of the measurement (given by the inverse bandwidth). Then inhomogeneous field distributions should not affect the frequency response provided that all carriers generated at the front contact are extracted at the back contact (and the DOS distribution is spatially homogeneous).

B. Theory

We will solve the rate equations for charge carriers for the special case of TOF measurement configurations. As in the transient experiment we assume unipolar photocurrent carried by electrons (for hole conduction an analogous analysis applies) and trap-limited conduction at a dominant transport path near the mobility edge. With the appropriate transition rates—(1) band-to-band generation of mobile carriers, (2) trapping of mobile electrons, n_c, into localized states, $N(E)$, (3) reemission of trapped electrons, $n(E)$, to the transport path, and (4) recombination of electrons at the back contact—the rate equations for electrons at the transport path and in the trap states can be written as

$$\frac{dn_c}{dt}=G_0+G_1e^{j\omega t}-\int_{E_F}^{E_c}\frac{dn(E)}{dt}dE-\frac{n_c-n_d}{t_{\rm tr}} \tag{1}$$

and

$$\frac{dn(E)}{dt}=n_c v\sigma[N(E)-n(E)]-N_c v\sigma n(E)e^{-(E_c-E)/kT}. \tag{2}$$

G_0, G_1 are the dc and ac generation rates, $\omega=2\pi f$ the modulation frequency, n_d the dark equilibrium concentration of free carriers, $t_{\rm tr}$ is the free-carrier transit time, and N_c the effective DOS at the transport path. $v\sigma$, electron velocity times electron capture cross section, denotes the trapping rate coefficient where a ballistic capture process has been assumed. [In case of diffusive capture $v\sigma$ must be replaced by the appropriate expression $4(\pi\sigma)^{1/2}D$, D being the diffusion coefficient for electrons.] For simplicity the transport path has been assumed at the band edge E_c.

In the rate equations the spatial dependence has been neglected as is usually done for TOF experiments, here with even better justification because spatial inhomogeneities of free- and trapped-carrier concentrations are effectively smeared out within the time frame of the experiment by fast drifts of generated and reemitted free carriers in the applied field ($t_{\rm tr}\ll 1/\omega_{\rm max}$). In Eq. (1) a monomolecular recombination term has been assumed. This may be questioned for volume recombination (e.g., in case of coplanar contacts) but for sandwich contacts the volume recombination time is larger than the transit time; then the free-carrier lifetime is terminated by recombination at the back contacts and is given by the free-carrier transit time

$$t_{\rm tr}=d^2/(\mu_0 V) \tag{3}$$

with the sample thickness d, mobility μ_0 at the electron transport path, and applied bias voltage V (for homogeneous field distributions).

Stating a solution of the rate equations for the carrier density at the transport path

$$n_c=n_{c,0}+n_{c,1}e^{j\omega t}$$

with the dc component

$$n_{c,0}=G_0 t_{\rm tr}$$

and the modulated component

$$n_{c,1}=|n_{c,1}|e^{-j\phi(\omega)},$$

the rate equations are solved exactly for the phase shift $\phi(\omega)$ and amplitude $|n_{c,1}(\omega)|$ of the modulated free-carrier density (and thus for the modulated component of the photocurrent which is proportional to $n_{c,1}$). A detailed derivation has been given by Oheda.[10] Using zero-

temperature approximation, the expression for the phase shift reduces to

$$\tan\phi(\omega)=[\omega+\pi kTv\sigma N(E_\omega)]\tau_\omega \tag{4}$$

and for the amplitude

$$|n_{c,1}(\omega)|=\frac{G_1\tau_\omega}{[1+\tan^2\phi(\omega)]^{1/2}}\ , \tag{5}$$

where

$$E_{Fn}=kT\ln(N_c/n_{c,0})\ , \tag{6}$$

$$E_\omega=kT\ln(N_cv\sigma/\omega)=kT\ln(\nu_0/\omega)\ , \tag{7}$$

and

$$\tau_\omega^{-1}=t_{\rm tr}^{-1}+\int_{E_{Fn}}^{E_\omega}v\sigma N(E)dE\ . \tag{8}$$

(E_{Fn}, electron quasi-Fermi-level; ν_0, attempt-to-escape frequency; τ_ω, reduced electron lifetime.) E_ω denotes a frequency-dependent demarcation energy that separates states in thermal equilibrium with the transport path from those that are frozen in deep traps within the considered time window $t<1/\omega$ in analogy to the time-dependent demarcation energy in transient experiments.[11] τ_ω is a frequency-dependent reduced lifetime for electrons in analogy to the deep trapping lifetime in transient experiments: electrons trapped between E_{Fn} and E_ω do not contribute to the modulated photocurrent although they are reemitted to the conduction band, but on a longer time scale than the measurement. Thus they are considered "recombined" and the effective electron recombination rate is enhanced by the integral factor in Eq. (8).

If the integral in Eq. (8) is small compared to $1/t_{\rm tr}$, the density of states is given by

$$N(E_\omega)=\frac{\tan\phi(\omega)}{t_{\rm tr}v\sigma\pi kT} \tag{9}$$

[ω in (4) can be neglected for $\omega<10^6$ Hz]. With knowledge of $t_{\rm tr}$, $v\sigma$, and ν_0 the DOS can be determined from phase-shift data on an absolute scale using Eqs. (9) and (7), where E_ω is the distance to the electron transport level E_c. In general, the relative DOS distribution $\tau_{\omega 0}v\sigma N(E_\omega)$ is obtained by recursion of Eq. (4), where $\tau_{\omega 0}$ is a minimum reduced lifetime at the smallest measured modulation frequency ω_0.[10]

C. Spatial resolution

In sandwich configuration the experimental sensitivity at a distance x from the front metal interface is given by the integrated absorption profile of the excitation light, assuming a homogeneous field distribution. Furthermore it is weighted by the relative current contribution of a photocarrier after reemission from a trap at the distance x from the front contact with respect to its total contribution, i.e., the distance from x to the back contact divided by the Schubweg, the total travel distance from the place of generation to the back contact (approximately equal to sample thickness d). In Fig. 1 we have plotted the sensitivity profile for the two wavelengths that we have used in our experiments as light sources.

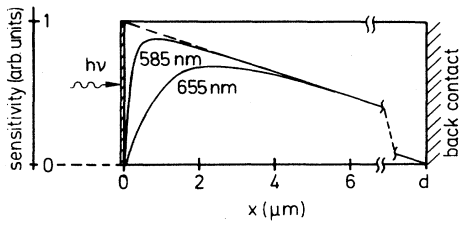

FIG. 1. Sensitivity profile in the case of a homogeneous field distribution. Maximum sensitivity is at $x\approx 0.2$ μm for a modulation light wavelength $\lambda=585$ nm and at $x\approx 1.5$ μm for $\lambda=655$ nm.

The experiment is performed in the low-intensity regime where the modulated injected charge is small compared to the external charge of the sample capacitance,[9] in other words, field distributions $\Delta F(x)$ due to the modulated charge can be neglected compared to the existing (externally applied or built-in) field $F(x)$. For inhomogeneous field distributions $F(x)$, produced by an externally applied dc voltage or the built-in field at the Schottky front contact, the sensitivity is modulated by an additional factor $1/F(x)$, since the number of trapped carriers at x is proportional to the free-carrier density $|n_{c,1}(x)|$ and from current continuity $|n_{c,1}(x)|\sim 1/F(x)$. Then

$$S(x)=[F(x)]^{-1}(1-e^{-\alpha x})(1-x/d)\ . \tag{10}$$

For near-interface absorption an average DOS from the interface to the back contact is obtained, for larger absorption depths and/or large fields at the interface the interface region is screened out and the bulk DOS can be deduced. In principle, by measuring with a number of different wavelengths the measurements can be deconvoluted and a spatial as well as energetic profile of the DOS is obtained.

In sandwich samples the ratio of electron-to-hole contribution to the sample response is given by the ratio of their Schubweg, their respective distance to contacts after generation. Care has to be taken not to use light with too large absorption depths compared to the sample thickness in order to keep the contribution of the other carrier species small with respect to the one that is studied. If the light is absorbed close to the contacts either only electrons or holes contribute to the signal, depending on the direction of the applied field. As in the TOF experiment either the gap-state distribution above or below E_F can then be determined.

Since the top Schottky contact is reverse biased during the measurements, a deep depletion region extends into the sample with a quasi-Fermi-level E^* approximately at or below midgap.[12] Within this depletion region states above E^* are essentially empty and modulatable. Therefore, in this region the deduced DOS should be reliable down to E^* that is about 0.9 eV below E_c in a-Si:H. Since the maximum sensitivity is kept in a range less than 2 μm away from the top interface by suitable choice of modulation wavelengths, the presented data in the following sections are measured in the deep depletion region and should be reliable in the given ranges.

III. RESULTS

A. Attempt-to-escape frequency

In order to obtain the energy scale for $N(E_\omega)$ the attempt-to-escape frequency ν_0 has to be determined. Figure 2 shows typical phase-shift data obtained on a 12 μm thick sample with semitransparent Cr front contacts for several different temperatures. (Data of 20 points/decade were taken with an average procedure of 10 measurements per point. The resulting curves were smooth as in the figure, no scatter of data points occurred.) The phase-shift curves show thermally activated behavior. $\tau_{\omega 0} v\sigma N(E_\omega)$ has been plotted against the modulation frequency and the frequency where the gap-state density shows a peak has been plotted versus $1/T$ (Fig. 3). From the slope of the Arrhenius plot, an activation energy of 0.66 eV for the peak has been deduced, whereby within the considered temperature range no shift in energy of the transport path and no thermal activation of the capture cross section is assumed. From Eq. (7) ν_0 has been determined to be 10^{13} Hz. Taking into account the explicit weak temperature dependence of $\nu_0 = N_c v\sigma \sim T^2$, the activation energy must be corrected by subtracting $2kT_m$ from the measured slope for E, where T_m is the average temperature of the Arrhenius plot.[13] Then, $\nu_0 = 2\times 10^{12}$ Hz. In general, ν_0 was found in the range $(2-10)\times 10^{12}$ Hz. This agrees favorably with similar measurements where thermally activated release times of electrons have been taken to determine ν_0 (e.g., deep-level transient spectroscopy measurements[13]).

B. Measurement parameters

1. *Applied voltage bias*

In general, thick a-Si:H samples (>5 μm) with semitransparent front contacts (Cr, Au, Pd) have been used for the measurements. The blocking nature of the contacts has been verified for the range of applied voltages by measuring the dc photocurrents and dark currents. They were independent of voltage indicating reverse saturation currents and only primary photocurrents.

For average values of capture cross sections $\sigma = (1-5)\times 10^{-15}$ cm^2,[14] $N(E) = 10^{16}$ eV^{-1} cm^{-3} around midgap, and $v = 10^7$ cm/s, the simplified equation (9) is valid provided that the free-carrier lifetime $t_{tr} < 20$ ns.

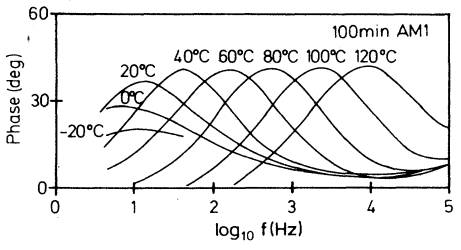

FIG. 2. Phase response of a 12 μm thick sample after 100 min of light soaking, measured on sandwich contacts at various temperatures.

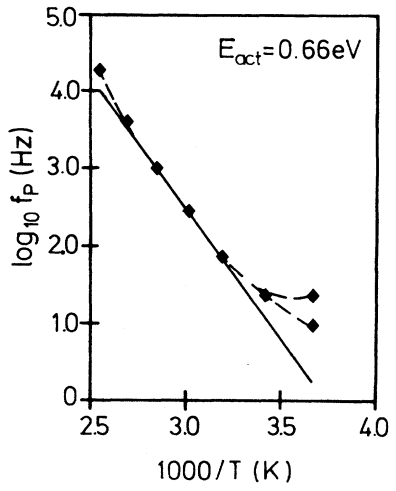

FIG. 3. Thermal activation energy of the DOS peak deduced from phase data in Fig. 2.

This is the case for an applied bias in the range of a few volts [from Eq. (3) with $\mu_0 = 10$ cm^2/V s]. In Fig. 4 phase-shift data of a sample after 2-h light degradation are shown for several applied voltages. To ensure homogeneous field distribution in the sample, a voltage step was applied a few μs before taking a measurement. In Fig. 5 the relative DOS is shown calculated from Eq. (4) and with the simple expression [Eq. (9)], respectively. For large bias the curves are nearly identical, indicating that the reduced electron lifetime is dominated by the transit time and Eq. (9) is valid. For small bias the curves show deviations that become larger with decreasing E_ω $(=E_c - E)$, reflecting the growing influence of the effective lifetime reduction with increasing integration limits $E_\omega - E_{Fn}$ in Eq. (8). The same effect is seen in Fig. 6. For large bias $\tan\phi$ increases proportional to V^{-1} $(\sim t_{tr})$ as predicted by Eq. (9). For sufficiently small bias the transit time becomes too large and the integral in Eq. (8) begins to dominate the effective lifetime τ_ω resulting in a now sublinear increase of $\tan\phi$ with V^{-1} as given by Eq. (4). This good quantitative agreement between theory and experimental results clearly demonstrates the applicability of the derived phase-shift analysis within the experimental boundary conditions.

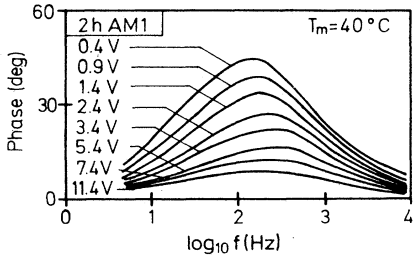

FIG. 4. Phase response of modulated photocurrents for several applied bias voltages.

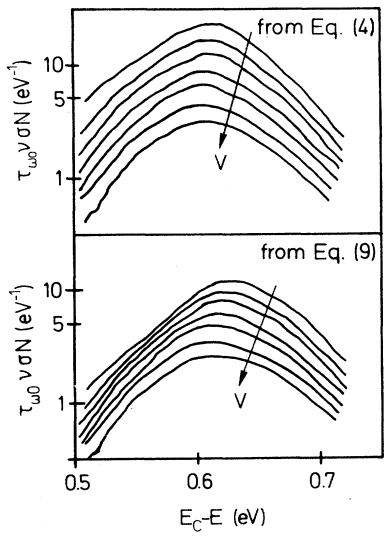

FIG. 5. Gap-state distribution $N(E)$ deduced from phase-shift data in Fig. 4 by use of the exact solution [Eq. (4)] and the approximate solution [Eq. (9)].

2. *dc versus pulsed voltages and absorption profile of the modulated light: Influence on spatial resolution*

When applying a dc voltage the sample is allowed to relax and an inhomogeneous field distribution $F(x)$ will build up with large fields close to the Schottky interface. For spatial sensitivity Eq. (10) applies. Phase-shift data taken with applied dc voltages turned out to be nearly identical to those with pulsed voltages in case of annealed samples (Fig. 7)—except that the dc voltages had to be larger to obtain the same phase response, which simply reflects the longer transit time for inhomogeneous field distributions. This is consistent with (4) in Sec. II A, that in case the time scale of the experiment (reemission time of electrons) is long compared to the transit time the field

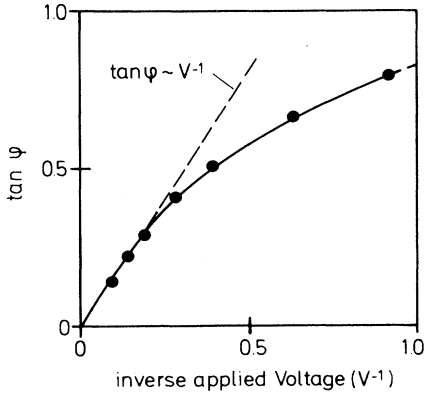

FIG. 6. tanϕ of the phase-shift peaks as a function of applied bias voltages (Fig. 4). In the linear range (large bias) the effective lifetime is terminated by t_{tr} and the approximate solution [Eq. (9)] is valid.

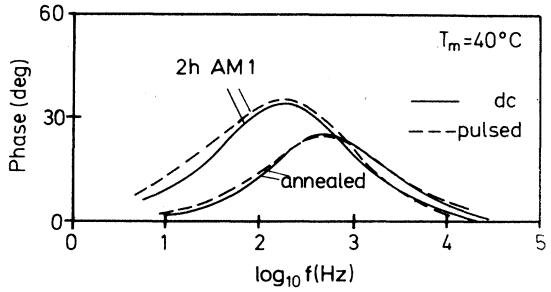

FIG. 7. Phase response for an applied voltage bias just a few μs before the measurement is taken (dashed lines) and for a dc bias (solid lines).

distribution should not matter for the phase response for a spatially homogeneous DOS—in contrast to TOF experiments, where the carrier transit that depends on actual field distributions is monitored directly.

After 2 h light degradation (AM1 illumination, ELH lamp, 100 mW/cm^2), the phase response was measured again (Fig. 7). Now a somewhat larger phase shift—particularly at small frequencies—was found in the case of pulsed voltages. The corresponding gap-state distributions are shown in Fig. 8, with the larger DOS determined for pulsed voltages. According to Eq. (10), in the case of applied dc voltages the spatial sensitivity is changed with more emphasis on the bulk region. The increased DOS for pulsed voltages then reflects the stronger defect creation close to the sample surface. This is expected for a given absorption profile of the degradation light source with decreasing light intensity into the sample.

Similar results are obtained when changing the spatial sensitivity by use of different wavelengths of the modulation source (Fig. 1). In Fig. 9 phase-shift data for the annealed sample and after light degradation are shown. The data were taken with a dc bias of 1.4 V and with wavelengths of 585 and 655 nm. The differences in this case are larger than for dc versus pulsed voltages. Even in the annealed case a slightly higher density of states is found near the sample-metal interface. We also note that

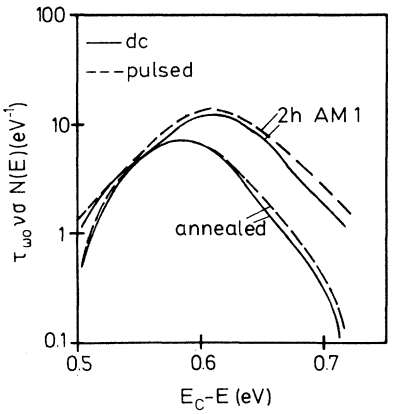

FIG. 8. Gap-state distribution deduced from phase-shift data in Fig. 7.

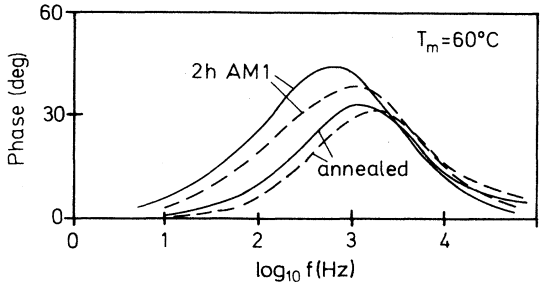

FIG. 9. Phase response for modulation light wavelengths of 585 nm (solid lines) and 655 nm (dashed lines).

the DOS peak is shifted deeper into the gap at the interface (Fig. 10); this point will be discussed in detail in the next sections.

From the above results it is concluded that the field variation by dielectric relaxation is not that large to change the sensitivity to a remarkable extent compared to variation of absorption profiles. In the following sections all results presented were measured with a dc voltage of 1.4 eV. We have checked our conception of spatial sensitivity further by degrading the sample with light of different absorption profiles. Using, e.g., an AM1 source and blocking contributions above 660 nm by an infrared filter we did find an increase of the DOS near the surface (measuring with 585 nm) whereas no detectable difference has been seen in the bulk (measuring with 655 nm). On the other hand, when the samples were degraded by light above 660 nm, an increase of the peak was found near the surface as well as in the bulk.

3. *Average light intensity and measurement temperature*

Due to the high signal-to-noise ratio the average excitation G_0 could be kept as low as 10^{10}–10^{11} photons/cm^2 s. The resulting photocurrents in the order of 10 nA/cm^2 were lower than the reverse saturation currents in the dark above room temperature, therefore deviations from thermal equilibrium can be neglected and $E_{Fn} \approx E^*$ (around midgap). In this range the phase shift and resulting DOS was found independent of the excitation level over 2 orders of magnitude. For higher excitation levels, or a lower temperature, the photocurrents exceed the dark current resulting in a shift of E_{Fn} away from E^*. According to Eq. (6) E_{Fn} depends logarithmically on G_0 and linearly on temperature. Then from Eqs. (8) and (4) an increase of τ_ω and correspondingly of the phase shift is expected with rising G_0 or falling temperature in qualitative agreement with the experiment. This enhancement with falling temperature can be seen, e.g., in Fig. 19 in addition to thermal activation of the phase-shift peak.

Another complication arises, when at sufficient excitation levels E_ω comes close to or even below E_{Fn} for small ω. In this range the derived phase-shift analysis is not valid, but in our measurements care was taken not to run into this regime.

C. Defect kinetics

1. *Defect creation*

The light-induced degradation (Staebler-Wronski effect) of undoped a-Si:H has been studied on sandwich samples of sufficient thickness (>4 μm) with semitransparent Schottky front contacts. The samples were annealed at 175 °C for 1 h and then were exposed to AM1 illumination at a fixed temperature below 95 °C. The phase shift was measured after different illumination times and the relative DOS distribution was calculated using Eq. (4) and $\nu_0 = 10^{13}$ Hz. For illumination at 60 °C the resulting DOS is shown in Fig. 11 with $E_\omega = E_c - E$. For the annealed sample a small peak at $E_c - 0.56$ eV occurs. The peak increases and shifts towards midgap with increasing illumination time. Integrating the area under the curve and plotting it versus illumination time, an increase of the total defect density with $t^{1/3}$ is found before the curve

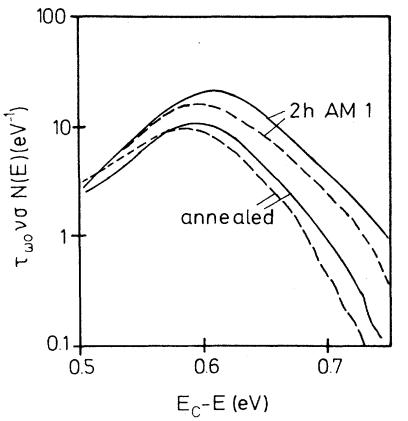

FIG. 10. Gap-state distribution deduced from phase-shift data in Fig. 9.

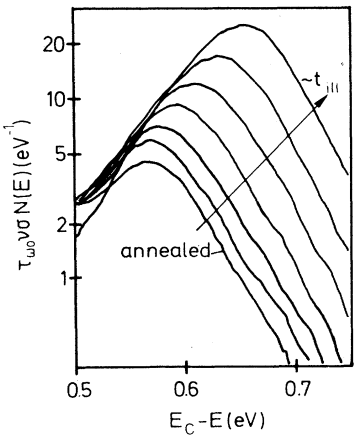

FIG. 11. Change of the deep-state distribution with AM1 illumination (t_{ill}=0, 2, 6, 18, 54, 150, and 990 min).

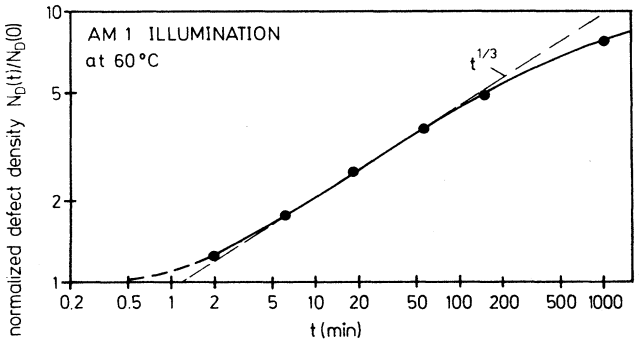

FIG. 12. Increase of the total density of deep states with illumination time.

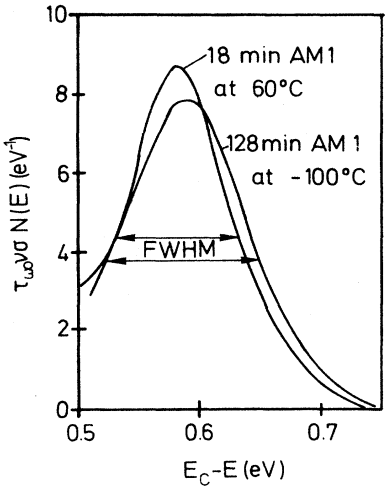

FIG. 13. Gap-state distribution after light soaking at different temperatures.

levels off into saturation (Fig. 12). Comparing total defect densities from light soaking at different temperatures, the apparent defect creation efficiency seems to be thermally activated with a small activation energy of about 30 meV in the temperature range $-100\,^{\circ}C$ to $+90\,^{\circ}C$. A similar value has been found for creation of spin centers by light soaking.[8] However, from amplitude measurements of modulated photocurrents, there is evidence that much more defects are created at low temperatures, but are annealed away when heating the sample to the measurement temperature ($=60\,^{\circ}C$ for phase-shift analysis) (see the Appendix). This suggests that creation of defects at a certain temperature is always accompanied by back annealing of defects that are unstable at this temperature. The net result of this effect is an approximately temperature-independent defect density, when measuring the defect peak at experimentally accessible temperatures (above room temperature).

The remaining small temperature dependence may be due to the temperature dependence of $\mu\tau$ products: Since defect creation is due to trapping or recombination of excess carriers at a potential defect site, there will be fewer accessible sites at lower temperatures because the mobility-lifetime product of excess carriers is thermally activated.[15] This will have two effects on the defect creation: first, the creation efficiency is proportional to the available sites during a carrier lifetime and thus will be also thermally activated with the same activation energy; second, actual sites are selected according to energetic preference (close to E_c) and according to spatial accessibility. The restricted availability of energetically favored sites at lower temperatures will then result in a broader defect distribution and a shift of the defect peak deeper into the gap. This has in fact been measured and is shown in Fig. 13.

2. *Defect annealing*

For annealing experiments we have degraded the samples by AM1 illumination at $60\,^{\circ}C$. The degraded samples were then annealed at fixed temperatures $>110\,^{\circ}C$ and the phase-shift data were taken after different anneal times at a fixed temperature below $90\,^{\circ}C$. Figure 14 shows how the defect peak is quenched with increasing anneal time: defect states located deeper in the gap are annealed first and—contrary to defect generation—the remaining defects tail off exponentially towards E_F with a slope kT where T is about the anneal temperature T_A. This has been verified for anneal temperatures from $120\,^{\circ}C$ to $170\,^{\circ}C$. In Fig. 15 two peaks with the same total density are compared—one caused by illumination of an annealed sample, the other by annealing of the same degraded sample. Again we see for the annealed case an exponential slope of kT_A whereas the other peak tails off somewhat slower. This shows that the annealing process is very selective concerning the energetic positions of the defects whereas the generation process produces a somewhat broader distribution.

The fact that the slope of the defect tail is equal to kT_A

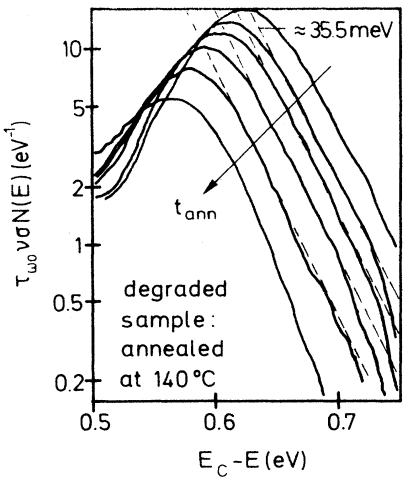

FIG. 14. Change of the gap-state distribution with annealing at $140\,^{\circ}C$ ($t_{ann}=0$, 5, 15, 45, 135, and 405 min after 125-min AM1). The exponential slope of 35.5 meV corresponds to the anneal temperature kT_A.

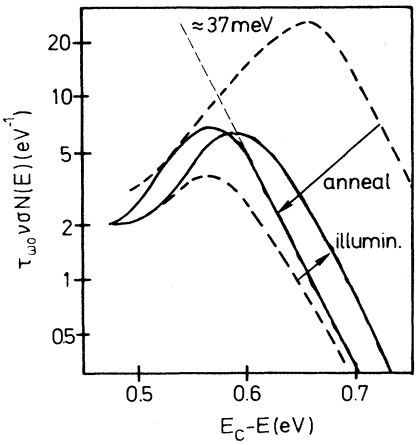

FIG. 15. Gap-state distribution after 8-min AM1 illumination of an annealed sample and after 30 min annealing at 160 °C of the same but degraded sample. The annealing process appears to be more selective with preferential annealing of the deeper states.

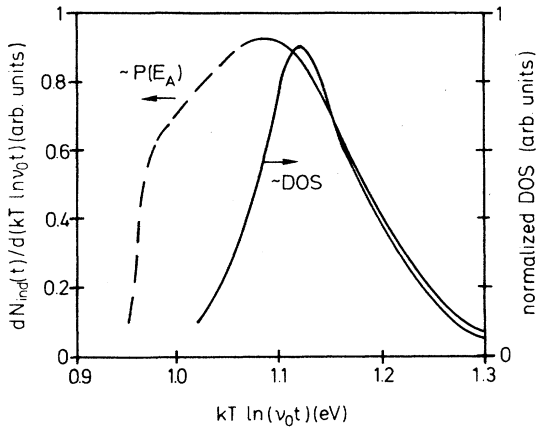

FIG. 17. Distribution of activation energies for annealing, $P(E_A)$, obtained as the derivative of the curves in Fig. 16, and the gap-state distribution, plotted vs distance to the valence band, after 990-min AM1.

suggests a correlation between the energetic positions of defects and their activation energies for annealing. To test this we have proceeded according to a method used by Stutzmann and co-workers to determine the activation energy distribution $P(E_A)$ for annealing.[8] We have measured the relative decrease of light-induced defects $N_{\text{ind}}(t)/N_{\text{ind}}(0)$ with annealing times for several different anneal temperatures and plotted this ratio as a function of $kT_A \ln(\nu_0 t)$ where $\nu_0 = 10^{10}$ Hz has been assumed, a value which gave the best possible overlap of the curves from different anneal temperatures (Fig. 16). Taking the derivative of this function yields the relative activation energy distribution $P(E_A)$, shown in Fig. 17, in case of a monomolecular annealing process. For comparison we have included the normalized defect distribution after long-time degradation plotted versus distance to the valence band (assuming a band gap of 1.8 eV). Particularly for the long anneal time tail with activation energies

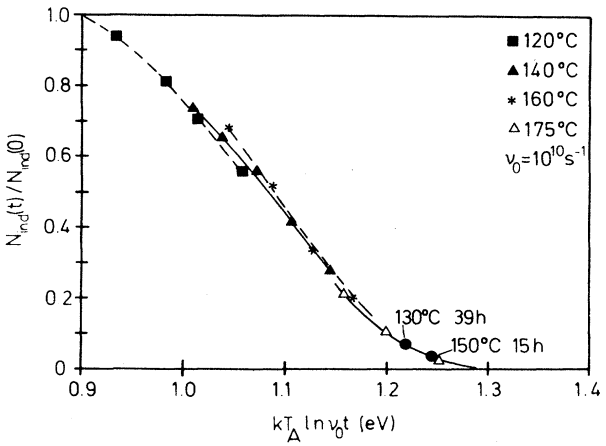

FIG. 16. Decrease of the light-induced defect density $N_{\text{ind}}(t)$ with annealing time t as function of $kT_A \ln(\nu_0 t)$ for various annealing temperatures T_A.

> 1.1 eV the relative defect distribution is proportional to the activation energy distribution within experimental error. This leads to the conclusion that at least for the more stable defects with larger activation energy the annealing process may be coupled with thermal emission of a valence-band electron into the defect. The reason why $P(E_A)$ deviates from the defect distribution for smaller energies is not entirely clear. An explanation might be the increasing experimental uncertainty in determination of $N_{\text{ind}}(t)$ for short anneal times and low anneal temperatures. For short anneal times the heat-up and cool-down times between anneal and measurement temperatures are in the order of the anneal times and will alter the results yielding a larger decrease of N_{ind} at short times and thus a larger contribution of smaller activation energies. On the other hand, similar activation energy distributions have been published by Stutzmann *et al.*,[8,16] where $N_{\text{ind}}(t)$ was directly monitored at the anneal temperature by ESR, and they found also a larger contribution of small activation energies. So there may be other effects that lower the activation energy or the annealing process is not monomolecular.

In case of monomolecular annealing kinetics

$$dN_{\text{ind}}(t)/dt = -RN_{\text{ind}}(t) \tag{11}$$

(R: decay constant) the decay can be transformed into a normalized form

$$dn(t)dt = -Rn(t)$$

where

$$n(t) = N_{\text{ind}}(t)/N_{\text{ind}}(0) \; . \tag{12}$$

Then the decay is independent of the initial density of induced defects $N_{\text{ind}}(t)$. In contrast, for bimolecular annealing kinetics the normalized decay is given by

$$dn(t)dt = -[RN_{\text{ind}}(t)]n(t) \ . \quad (13)$$

In this case the decay "constant" is always proportional to the defect density $N_{\text{ind}}(t)$. We have measured the relative decay of $N_{\text{ind}}(t)/N_{\text{ind}}(0)$ for three different initial defect densities shown in Fig. 18, and within experimental error we do find the initial decay rate to be proportional to the initial defect density, in contrast to ESR results,[8,16] where a definite monomolecular annealing process has been determined. After the initial decay, however, the process changes into a monomolecular one. This is seen in Fig. 18: the decay rate (slope) becomes independent of the actual defect density after about 50 min. Interpreting the data of Fig. 18 in terms of monomolecular versus bimolecular behavior, however, some caution is in order. As has been shown in Fig. 11, higher initial defect densities are also associated with a shift of the defect distribution deeper into the gap and thus probably with a larger contribution of defects with small annealing activation energies. The initial decay in Fig. 18 is therefore increased in case of larger initial defect densities. On the other hand, the deduced distribution $P(E_A)$ is compared with the largest initial defect density distribution after 990 min AM1 and still shows strong deviations for smaller activation energies. Thus, for higher densities of induced defects the annealing kinetics may be changed with the effect of lowering the potential barrier for defect annealing.

As mentioned in the preceding section the annealing of created defects is intimately connected with the temperature of degradation. We always obtained a partial annealing of defects when storing the sample above degradation temperature, although below 90 °C. On the other hand, when degrading the sample at 60 °C, even long storage (3 days) at 60 °C did not result in a partial annealing of the created peak. These observations are consistent with annealing characteristics from photoconductivity measurements where a partial recovery of the annealed state photoconductivity was found when the sample was stored above degradation temperature but no annealing was seen when storing at the degradation temperature.[17] The steepest tails of the remaining defect peak were found when the sample was degraded at −100 °C and annealed at 60 °C for 3 days. When measured at 50 °C the characteristic slopes were about 33–34 meV for near-interface states (585-nm modulation light) and about 29 meV for states deeper in the bulk (655-nm modulation light). For states in the depletion region there seems to be an upper limit for the tail slope whereas for bulk states the exponential slopes were directly correlated with the actual anneal temperature down to the experimentally accessible temperature of 60 °C.

At present the reason for an upper limit of the measured slopes near the interface is not clear. However, the finite spatial resolution (Fig. 1) together with a band bending in the space-charge region (presumably a shift of the defect peak according to the band bending) may result in a smaller apparent slope. Another reason may be a broader transport path at E_c close to the interface, limiting the resolution of the DOS distribution by the "sharpness" of the electron transport path (see next section).

From Fig. 13 we can understand phenomenologically why defect annealing takes place only for temperatures above the degradation temperature. The peak created at −100 °C and subsequently measured at 60 °C is broadened towards midgap compared to the one created at 60 °C. If it is right that the energetic position of a defect is correlated with its stability against annealing, the lower-lying defects of the peak produced at low temperature may be already annealed at 60 °C, which results in a partial annealing of this peak, whereas the peak produced at 60 °C has from the beginning only defects that are "stable" at this temperature.

3. *Shallow defects*

When phase-shift data are taken at low temperatures (−100 °C), according to Eq. (7) the distribution of shallow defects for $E_\omega = 0.25$–0.4 eV is obtained from the experimentally accessible frequency range. Figure 19 shows phase-shift data for low temperatures from −130 °C to −78 °C measured on a sample with semitransparent Cr front contacts. A thermally activated phase-shift peak is obtained, corresponding to a peak in the DOS at 0.35 eV below the electron transport path E_t (using $\nu_0 = 10^{13}$ Hz; a possible temperature dependence of ν_0 has been neglected; the energetic distance of the peak to E_c may be larger by about 50–100 meV due to the electron transport path

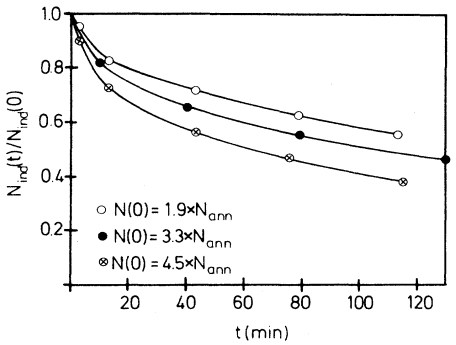

FIG. 18. Decrease of the light-induced defect density with annealing time t at 140 °C for three different initial defect densities.

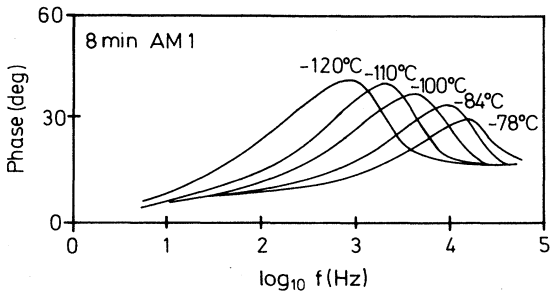

FIG. 19. Phase response of a 12 μm thick sample after 8 min of light soaking, measured on sandwich contacts in the low-temperature range.

being located in the conduction-band tail at low measurement temperatures. For a more detailed treatment see Refs. 6 and 7). The observed peak would be in agreement with a peak in the DOS detected by field-effect measurements at the same energy below E_c.[18–20]

In Fig. 20 the quenching of the shallow peak with light degradation is shown and in Fig. 21 two peaks with the same total defect density are compared—one produced by illumination of the annealed sample, the other by annealing of the light-soaked sample. Upon illumination a steep exponential tail towards midgap is found, and the states further from the conduction band are annihilated first. A somewhat broader defect distribution is found for creation of shallow defects during annealing. In contrast to the peak of deep states, here quenching is caused by illumination and a peak increase by annealing of the sample. On the other hand, a direct conversion from the measured shallow states to measured deep states can be ruled out since the time dependence for decrease of shallow states does not follow the $t^{1/3}$ law as determined for the increase of deep states. Also, an applied depletion bias during annealing produced an increase of both peaks, suggesting the involvement of other states—presumably below E_F—that are converted into the measured states above E_F (see below).

The exponential slopes of the shallow peak during quenching were determined between 23–30 meV. The apparent slopes, however, could not be well correlated with the sample temperature during illumination, but were strongly dependent on the measurement temperature (e.g., from 23 meV at −120 °C to 29 meV at −89 °C after 8-min AM1 illumination at 10 °C) and to a lesser extent on the intensity of the modulated light with larger slopes for higher light intensities. The reason for this is not completely understood. We note, however, that the electron hopping transport path at low temperatures in the tail is not energetically "sharp" but may be distributed with an exponential fall-off parallel to or steeper than the tail falloff.[21] Since the experiment is based on reemission of electrons from filled states (the defects) to the transport path, a convolution of the DOS distributions with the transport path is measured and the energetic resolution of the defect distribution is limited by the sharpness of the transport path. Thus, although the DOS peak may have steeper falloffs, the experimentally determined slope will be that of the transport path distribution, or in other words, that of the probability distribution for activation to a range of hopping transport levels in the tail at a certain temperature.

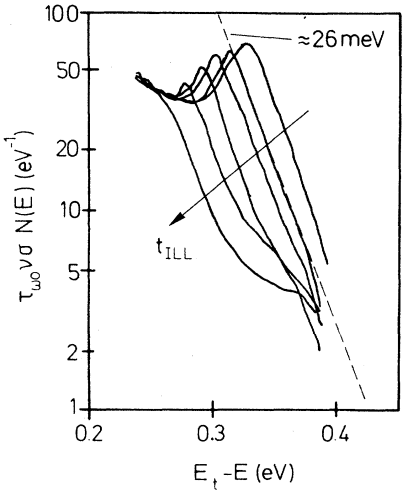

FIG. 20. Change of the shallow gap-state distribution with AM1 illumination (t_{ill}=0, 2, 8, 32, 128, and 1300 min). An exponential tail with a slope of 26 meV is obtained.

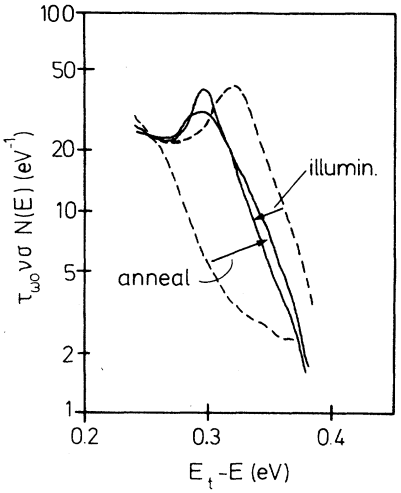

FIG. 21. Shallow-state distribution after 8-min AM1 illumination of an annealed sample and after 30-min annealing at 160 °C of the same but degraded sample. The degradation process appears to be more selective with preferential quenching of the deeper states.

For identical measurement conditions (temperature, modulation light intensity) a correlation was found with steeper slopes and larger shifts of the shallow peak towards E_c for higher temperatures during light soaking. The quenching efficiency increased rapidly for lower degradation temperatures, but the quenched-in states was not stable for temperatures above the degradation temperature. For instance, the shallow peak completely disappeared after only 8 min of AM1 illumination at −100 °C but recovered completely after heating the sample to 60 °C for 10 min. Even after long degradation (130 min at −100 °C), after which a large peak of deep states remained stable at 60 °C, the shallow defect peak recovered completely although with a broader distribution. Again, this suggests a nearly temperature-independent quenching process upon illumination paralleled by a strongly temperature-dependent restoration of shallow defects.

4. Bias annealing

When samples with Schottky front contacts are annealed with a depletion bias of 10–20 V, a metastable increase of both—shallow and deep state—peaks is obtained (Fig. 22). Both peaks are relatively stable and can be annealed only above 100 °C. In contrast to the light-soaking experiment, the maximum of the deep-state peak does not shift significantly towards midgap, and from amplitude measurements of modulated photocurrents at low

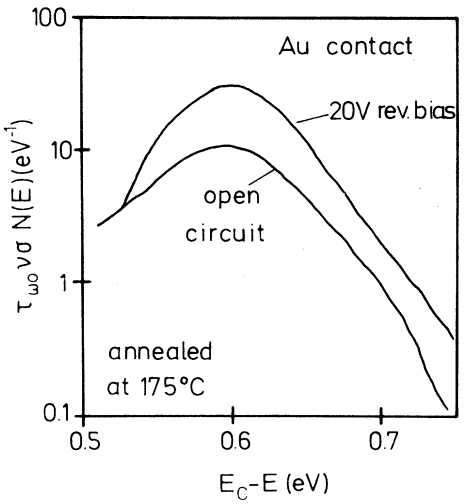

FIG. 22. Deep-state distribution after annealing with open circuit and with 20-V depletion bias. A similar increase of the gap-state density has been found for the shallow state peak.

temperatures there has been no evidence that the total density of deep states does change upon bias annealing (see the Appendix). This suggests that along with the increase of deep states above midgap a decrease of deep states below midgap must occur such that the total of deep trapping and recombination centers does not change significantly. We note the similarity to results obtained from bias annealing experiments on doped samples by means of sweep-out techniques.[22]

Another important result is obtained concerning the spatial dependence of shallow defects. When annealing without bias, the shallow peak occurs only in the depletion region of the Schottky contact (measured by 585-nm modulation light with maximum sensitivity about 200 nm below the interface). For distances >1 μm from the interface (655-nm modulation light) no or only a small shallow peak is obtained. However, when annealing under depletion bias, the peak near the interface is increased and below 1 μm a shallow peak of a similar size occurs. We conclude therefore that spatial differences in the defect distribution of annealed samples—concerning the two measured peaks—are not due to structual inhomogeneities near the interface but mainly to the electronic occupation functions during annealing. We believe this is also the reason for spatial inhomogeneities of the deep-state peak that is shifted towards midgap near the interface (Fig. 9).

The increase of defect peaks is accompanied by a metastable 20–40 fold increase of dark current (at 60 °C for 10 V bias). This indicates a shift of the dark Fermi level near the interface towards E_c, thus lowering the barrier for injection of electrons. (A metastable change in the band bending profile near the interface has been verified by TOF experiments on the same sample.) A Fermi-level shift, however, should be expected from our results of a defect increase above midgap and a decrease below midgap since the Fermi level must readjust for charge neutrality to compensate for the higher defect density above midgap.

IV. DISCUSSION

From spatial resolution of the DOS it was found that the deep states are also generated deep in the bulk more than 1 μm from the interface (and the spatial DOS profile was correlated with the absorption profile of the degradation light). This is in agreement with recent measurements by Kočka and co-workers[23] on *p-i-n* junctions where a Fermi-level shift associated with the Staebler-Wronski effect (SWE) in the intrinsic bulk region was measured by ac conductivity and on *n-i-n* structures[24] where this shift and an increasing peak at $E_c-0.61$ eV has been determined by temperature-modulated space-charge–limited current (SCLC) measurements. Similar results have been obtained from studies of the thickness dependence of the SWE on coplanar samples.[25] In contrast, ESR signals were found to increase only in a region close to the interface (<1 μm).[8,26] The SWE as measured by ESR could be directly correlated with stress in the samples[26] as well as subgap absorption around 1 eV.[27] In contrast, the SWE as measured by photoconductivity[28,29] and by $\mu\tau$ products[27] does not show a correlation with applied stress or even is suppressed when applying large compressive stress.[30]

A. Defect structure

The observed differences of ESR and subgap absorption on one side, compared to photoconductivity, $\mu\tau$ products, Fermi-level shift, and our data on the other side suggest that there must be at least two light-induced defects and that the defects observed by ESR are different to those observed by modulated photocurrents. By interpreting the observed defect peaks as the positively charged Si atom with different hybridization states (D^+ with sp^3 bonding and $^*D^+$ with sp^2 bonding) we show that our results are explained in a consistent way and, moreover, many controversies in the literature concerning the gap-state distribution and defect kinetics are overcome.

Since both defects—D^0 and D^+—obey the same macroscopic creation kinetics (power law and thermal activation energy) the defect creation process is assumed to have the same origin for D^+ and D^0 centers, namely, photogenerated electrons and holes. Two defect creation processes have been proposed and both of them may apply: Weak bond breaking and creation of two metastable dangling bonds[8] or a process similar to that proposed by Elliott[31] and Adler[32,33] where $^*D^+$ and $^*D^-$ centers with 120° and 95° bond angles relax to the tetrahedral bond-angle configuration (109.5°) by trapping of electrons or holes, introducing deep dangling-bond states. We will discuss this in detail later.

Our experiment gives no direct information about the charge state of the measured deep defect center, it could be D^0 or D^+ in dark equilibrium with trapping and reemission of an electron during modulation. The steep exponential tails of the deep defect peak towards E_F upon

annealing, however, support the interpretation as D^+ states since trapping into D^0 should cause an additional broadening of the resulting D^- distribution that is due to a distribution of effective correlation energies, which is expected for amorphous materials such as *a*-Si:H. In addition, signals originating from possible D^0 states are suppressed by the ratio of capture cross sections $\sigma_{D^0}/\sigma_{D^+}$, since the trapping rate into a particular defect and thus the modulated photocurrent signal is proportional to the defect density times the associated capture cross section [see Eq. (4)].

For our further analysis we adopt the thermodynamical model for defect formation developed by Bar-Yam and co-workers together with their theoretical calculations of the dangling-bond correlation energies in *a*-Si:H. According to them the actual DOS is established by freeze-in of a thermodynamical equilibrium defect structure when cooling the sample below a transition temperature T^*. If a particular defect has small or negative correlation energies and if a pool for potential defects with a fairly wide energetic distribution in the band gap exists—as for the Si-DB in a typical distorted host structure of *a*-Si:H (Ref. 4)—annealing will result in a peak of D^+ centers above and D^- centers below the Fermi level and roughly exponential tails of the defect distribution towards E_F.[5] Positive correlation energies tend to suppress the states introduced by the corresponding charged defects and only a peak of D^0 centers is established at about $E_F - U/2$ during freeze-in. According to their calculations potential sites for DB's with positive correlation energies occur only at strongly distorted host sites which should be directly correlated with strains in the material. Thus, D^0 states in unstrained regions are suppressed during freeze-in of the defect structure, whereas the formation of D^- is enhanced in these regions. On the other hand, the formation of D^+ should not be affected by strains since no correlation energy is defined between D^0 and D^+ states. Thus, D^+ may be formed in strained as well as unstrained regions.

This is in full agreement with experimental findings: D^0 centers from ESR were found only in regions with mechanical stress. In high-quality samples of annealed undoped *a*-Si:H the spin signal increased at the most by a factor of 2 for a sample thickness variation from 0.1 to 1 μm and did not increase any further in the range 1 to 10 μm which is clearly seen in Fig. 2 of the paper of Stutzmann *et al.*[8] Even after light degradation using light with homogeneous absorption throughout the films an increase by a factor of 10 was observed only within the first μm of the samples. The sensitivity profile for creation of D^0 centers could be directly correlated with the mechanical stress profile in the films (internal and external stress), in unstrained regions there was no increase of spin signals upon illumination. As mentioned above, similar results have been found from subgap absorption (detecting D^0 and D^-) whereas no correlation with stress was found from photoconductivity and $\mu\tau$ measurements (detecting D^+ which should act as very efficient centers for electron capture). In this context it is interesting to note recent results for the correlation energy U of the defect center by combined ESR, subgap absorption, and transport measurements determined to $+(0.2\pm0.1)$ eV.[34] This result comes close to the calculated values of largest DB correlation energies in a distorted host.

The metastable increase of the measured defect peaks along with the deduced shift of the equilibrium Fermi level towards E_c after depletion bias annealing strongly supports their positive charge state in the dark as well as a thermodynamical model for defect formation. According to Ref. 5 the forced downward shift of the Fermi level by the depletion bias should enhance the formation of positively charged states above E_F due to a corresponding decrease of the formation energies whereas neutral states should not be affected and the formation of negatively charged states below E_F should be suppressed. The quenching of states below E_F has been deduced from amplitude measurements (see the Appendix) and was directly measured on pin structures.[35] We would like to stress that the observed peak enhancements above E_F are inconsistent with the interpretation of the deduced deep peak as due to negatively charged DB's with a positive correlation energy of 0.3–0.4 eV. Given that case, with bias annealing we should find either no change of the peak according to Ref. 5 since the equilibrium state would be D^0, or quenching according to observations in Ref. 35. Also, the equilibrium Fermi level would have shifted towards midgap contrary to observations.

Our results suggest a DOS model as shown in Fig. 23. In the annealed state the deep defect density (D^+, D^-, and in strained regions D^0) is small and a large number of threefold coordinated $^*D^+$ and $^*D^-$ exist that are stable under dark thermal equilibrium conditions. Upon illumination excess electrons and holes may be trapped at $^*D^+$ and $^*D^-$ centers, creating unstable $^*D^0$ states that will rapidly relax into a neutral dangling-bond defect, D^0, with tetrahedral bond-angle configuration. Hereby are $^*D^+$ preferably converted into states above and $^*D^-$ into states below midgap.[33]

During illumination the created deep DB states are located between the quasi-Fermi-levels E_{Fn} and E_{Fp} and will be occupied according to ratios of respective capture

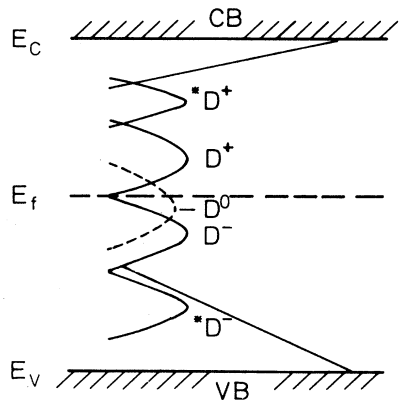

FIG. 23. Model of defect structure in undoped *a*-Si:H. The neutral state D^0 occurs only for defects with positive correlation energies in strained regions of the sample.

cross sections for electrons and holes.[36] Since capture cross sections of charged defects are larger than for neutral defects[14] there will be a certain fraction of neutral DB's between E_{Fn} and E_{Fp}. The D^0 centers may now be stabilized by further relaxation of the surrounding network or alternatively reconverted into $^*D^+/^*D^-$ centers by capture of a hole and electron and subsequent back relaxation of the bond angles. The relaxation processes may depend on the available thermal energy (sample temperature) during illumination and on the actual structure of the surrounding network such as strains and, correlated with this, hydrogen content and possibly impurities.

The temperature dependence of electronic occupation functions for defects together with a temperature-dependent stabilization and reconversion process for the created deep states is responsible for the observed temperature dependence of the quenching rates and energy shift of the shallow peak. At low temperature back annealing is small and the occupation of $^*D^+$ with electrons is large (E_{Fn} closer towards E_c for the same illumination level) resulting in a large effective quenching rate. On the other hand, at low temperature the created deep defects are not able to relax into a sufficiently stable position, therefore the shallow defects are restored when heating the sample to room temperature. When DB's are reconverted during illumination the created shallow defects may also be redistributed towards a lower energy state and a more stable configuration by relaxation of the surrounding network (e.g., spatially close $^*D^+$-$^*D^-$ pairs are expected to be more stable and their energetic position is shifted towards the band edges due to Coulomb interaction[33]). Thus, at higher temperatures with increasing ability of the network for structural relaxation a smaller effective quenching rate as well as a larger shift of the shallow peak towards E_c should occur which is experimentally observed.

As we have outlined before, the origin of the slopes for shallow defects is not completely understood but might be due to the exponential slope of the electron transport path in the conduction-band tail. If this is the case, an effect of light soaking at different temperatures on TOF signals should be seen with steeper conduction-band (CB) tails for higher illumination temperatures. Clearly, this point needs further investigation. Also, if there were an effect on the CB tail, it would suggest the involvement of weak bonds in the shallow-state–deep-state conversion process as well. This view is further supported by the fact that the shallow peak could not be detected in the bulk outside the depletion region although the creation of deep states is clearly observed more than 1 μm away from the Schottky interface.

Annealing of deep states in the dark obeys different conversion kinetics. Since reconverted shallow states should be stable in the dark there occurs only a one-way conversion of metastable deep states into shallow states. But in this case the deep states are charged according to their position with respect to the Fermi level and it has been shown that annealing is a very selective process for the D^+ states closest to E_F resulting in exponential tails towards E_F. If we assume a similar selective annealing process for D^- centers below E_F and if the observed shallow defects $^*D^+$ are reconverted from D^- states, then a broader peak of shallow states should be obtained.

To summarize, during illumination the selection for conversion is made with respect to the shallow states producing a broader peak of deep states and leaving a steep tail of shallow states. The reason may be that the deep states between the quasi-Fermi-levels are occupied according to capture cross sections and not according to their energetic position. Then there is no preference for reconversion with respect to energetic positions of the deep states. In the dark, however, deep states are charged and a sharp selection for annealing is made producing a broad peak of shallow states and leaving a steep tail of deep states.

Our experiments do suggest the involvement of states below E_F: bias annealing enhances both peaks above E_F; the time dependence for creation of deep states D^+ is different from that for quenching of shallow states, $^*D^+$; shallow states quenched at low temperatures recover almost completely at room temperature whereas the created deep states remain stable to a large extent; degradation by light soaking causes a Fermi-level shift towards midgap although the measured DOS above E_F increases. This all indicates conversion of $^*D^+$ centers into states below E_F, presumably D^-, with different creation and annealing characteristics than for D^+.

The deduced activation energies for the annealing of D^+ states E_A are correlated with the energetic position of D^+ in the gap and apparently is $E_A \approx E(D^+) - E_v$. This suggests that the rate-limiting step for annealing is the thermal emission of a valence-band electron into the D^+ state. Our results may be related with those from annealing experiments on a-Si:H (Ref. 16) and on deuterated a-Si:D (Ref. 37) where as rate-limiting step the emission of an electron from D^0 into the conduction band was suggested and a direct rate-limiting involvement of hydrogen in the conversion process was ruled out. Nevertheless, the possibility of indirect influence of hydrogen content by relaxing internal stress is still left open. We note that apparent similarities between hydrogen diffusion and annealing behavior[38] do not necessarily imply that annealing is coupled to the diffusion of hydrogen but rather that both processes may have the same origin, namely, thermal emission of electrons and holes from the respective band edges. Even if hydrogen were to passivate existing dangling bonds, according to our results the rate of passivation is clearly determined by the energetic position of dangling bonds in the gap and not by the availability of hydrogen. To put it in another point of view, the hydrogen diffusion rate may even be limited by the availability of DB's at a particular energetic position in the gap. When DB's are annealed according to the selective annealing procedure described before, less and less DB's with low potential barriers are available, resulting in the same time dependence for the diffusion rate as for the annealing rate. This has been observed.[38] In doped or compensated films the diffusion rate has been shown to be strongly correlated with the DB density.[39] This may be a further indication that hydrogen diffusion is controlled by DB's. We point out, however, that these speculations need to be reexamined in the context of pos-

sible microscopic migration and annealing mechanisms that have not been considered yet.

The reason why, for annealing of D^+, the emission of a valence-band (VB) electron is needed is not clear since trapping of a conduction-band electron should occur with much larger rates. The conversion D^+-$^*D^-$, however, involves a change of charge state by two electrons which might happen by simultaneous trapping of a CB electron and emission of a VB electron into the D^+ state. Then the annealing rate is limited by the less frequent emission of the VB electron. The emission of VB electrons might also be the reason for the low attempt-to-anneal frequency $\nu_0 \approx 10^{10}$ Hz compared to the attempt-to-escape frequency for emission of electrons from traps to the conduction band (determined to 10^{12}–10^{13} Hz).

Another question concerns the different stabilities of D^+ and D^- defects, i.e., why do states below E_F, D^-, convert easier into $^*D^+$ than when the annealing of D^+ takes place? If we assume in analogy that annealing of D^- is limited by emission of an electron into the conduction band, the annealing activation energy is given by $E_A \approx E_c - E(D^-)$. Since the position of D^- has been determined by various experimental methods to 0.9 eV below E_c the annealing process should have smaller activation energies, thus reconversion of $^*D^+$ occurs already at lower temperatures.

For a sufficiently high density or small spatial separation of D^+ and D^- the charged states may directly exchange an electron, then thermal emission of charge carriers is unnecessary and the annealing rate is either limited by the electron exchange rate or by subsequent trapping of the respective charge carriers. In both cases the annealing rate may be much higher yielding the observed "biomolecular" behavior for a large density of deep states.

The proposed conversion processes are consistent with electron-hole injection experiments[40] where hole injection was found to decrease mainly the $\mu\tau$ product and electron injection to enhance the 1-eV subgap absorption. In our model trapped holes convert $^*D^-$ into D^+ states that should act as very efficient electron recombination centers, and trapped electrons create D^- states below E_F thus enhancing the subgap absorption. Similar arguments apply to the Han-Fritzsche experiment:[41] According to their results, D^+ states created at low temperature remain to a large extent stable at room temperature and therefore decrease the measured $\mu\tau$ product whereas the less stable D^- states are annealed back into $^*D^+$ states, therefore no increase of 1-eV subgap absorption could be detected at room temperature. At last we want to note recent degradation studies of the gap-state distribution by a related technique, the frequency-resolved modulated photocurrent (MPC) spectroscopy.[42] In addition to the peak at $E_c - 0.6$ eV that increases upon light soaking, another peak at 0.6 eV above E_v has been detected that decreases with light soaking, which is in perfect agreement with the proposed $^*D^-$ peak.

V. SUMMARY

A novel experimental technique for measurements of modulated photocurrents over a wide frequency range has been applied to undoped a-Si:H and the phase-shift analysis of modulated photocurrents introduced earlier by Oheda has been further developed for the special case of contacts in sandwich configuration. Our experimental data yield the DOS distribution above the Fermi level up to about $E_c - 0.25$ eV. Without exact knowledge of capture cross sections $\sigma(E)$ and transit times absolute values for the DOS are not determined but the method has been proved to be very sensitive to the relative energetic distribution of gap states $N(E)$ [normalized by $\sigma(E)$] as well as to changes in the DOS distribution by degradation or annealing of the material.

Well-known results concerning the Staebler-Wronski effect like power laws for deep defect creation upon illumination or the distribution of annealing activation energies have been reconfirmed and additional insight in the conversion processes has been gained by linking creation processes and annealing activation energies to the energetic position of defects in the gap. The two DOS peaks determined at $E_c - 0.4$ eV and $E_c - 0.6$ eV are in agreement with results from various other experiments. We want to emphasize particularly the shallow peak originally measured by means of the field-effect technique but then questioned because of strong surface sensitivity and other shortcomings of this method. We have found that this peak occurs within the depletion region of a Schottky interface, but it has also been measured more than 1 μm away from the interface provided that the depletion region during annealing extends that far into the bulk. Therefore states due to interfacial defects are with all probability ruled out as the origin of this peak.

Our experimental results strongly support a picture of the defect structure in a-Si:H originally developed by Adler and put forth by Bar-Yam and co-workers. According to their model the shallow peak is due to Si^+ ions forming three sp^2 bonds and the deep peak originates in positively charged DB's. Our bias annealing experiments and measured Fermi-level shifts indicate an analogous distribution of negatively charged defects in sp^3 and p bonding configuration below the Fermi level. Based on thermodynamical considerations the actual formation or annihilation of charged defects out of a defect pool primarily depends on electronic occupation functions that in turn are given by illumination, depletion, or thermal equilibrium and to a certain extent on the structural relaxation ability of the surrounding network that is determined by available thermal or recombination energies as well as the specific structure itself (e.g., strains or hydrogen content). We should stress that the formation of a peak of D^+ states above the Fermi level is independent of correlation energies associated with D^0/D^- transitions of these states. Provided that potential energetic sites for the formation of this defect type are spread over a fairly wide range extending above E_F, the formation of D^+ centers above E_F will be always enhanced due to lowered formation energies. Positive correlation energies that could suppress the formation of D^+ centers cannot occur for the associated D^+/D^0 transitions. The annealing rate of D^+ centers seems to be limited by thermal emission of electrons from the valence band into the defect and not by the availability (diffusion rate) of hydrogen.

Within the framework of the outlined model a number of not satisfactorily understood and sometimes seemingly contradictory experimental results in the literature of the past years can be put on common grounds. Allowing a spread of effective correlation energies, depending on the distortion of the surrounding network, the SWE is both an interface and a bulk effect with formation of primarily charged centers in unstrained regions, i.e., in the bulk, and formation of D^0 only in strained or interface regions. Recognizing the D^+ centers above the Fermi level as main recombination centers for electrons, the persistent differences between ESR results on one side and $\mu\tau$ products and photoconductivity on the other concerning bulk, interface and stress effects are thus resolved. The observation of two distinct levels for D^- centers depending on the used experimental technique is understood within the context of small effective correlation energies. Experiments that detect a peak at $E_c-0.6$ eV usually work by inducing a nonequilibrium condition where D^+ centers above E_F are populated by electrons and a resulting effect—either reemission of electrons (e.g., in case of modulated photocurrents) or transport behavior (e.g., SCLC)—is measured and the result is interpreted as a peak of D^- states. We note that when the centers become populated only by one electron the experiment should yield the distribution of D^0 (D^+) states and when they are populated by two electrons, the result is a distribution of D^- states that exhibits an additional broadening due to a distribution of correlation energies. This may be the reason why for experiments with extremely low level excitation such as the modulated photocurrent measurement a sharp peak with steep tails is obtained whereas high-level injection or excitation with saturation of traps [e.g., SCLC (Ref. 22)] yield a broader peak of D^- centers.

APPENDIX: AMPLITUDE MEASUREMENTS

Amplitude and phase response are related by Eq. (5) and both contain, in principle, the whole information of the response behavior. An analysis of the amplitude response of modulated photocurrents has been introduced earlier by Niekisch,[43–46] but as pointed out by Oheda[10] there are certain limitations to this analysis. Also, from an experimental point of view, the amplitude response is an only gently varying function of frequency (Fig. 24) whereas phase-shift data show more structure that may be easier to analyze. Nevertheless, certain results are obtained in a more straightforward manner from amplitude data: They can, for instance, be used to derive directly the (relative) integrated density of states $\bar{N}$ between two demarcation levels $E_{\omega 1}$ and $E_{\omega 2}$. From Eq. (8) one obtains

$$\tau_{\omega 1} v\sigma \bar{N} = \tau_{\omega 1} v\sigma \int_{E_{\omega 1}}^{E_{\omega 2}} N(E)dE = \frac{\tau_{\omega 1}}{\tau_{\omega 2}} - 1 \ . \tag{A1}$$

This equation is especially useful for evaluation of changes in the total DOS as the total of deep states (D^+) by annealing or light soaking. The ratio of states before and after a treatment $\bar{N}/\bar{N}'$ is given by

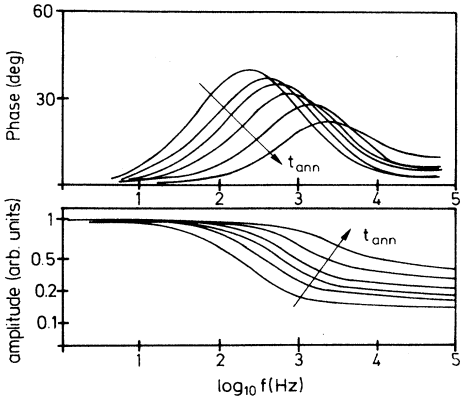

FIG. 24. Phase response and corresponding amplitude response of modulated photocurrents, measured after different annealing times.

$$\frac{\bar{N}}{\bar{N}'} = \frac{(\tau_{\omega 1}/\tau_{\omega 2})-1}{(\tau'_{\omega 1}/\tau'_{\omega 2})-1} \frac{\tau'_{\omega 1}}{\tau_{\omega 1}} \ , \tag{A2}$$

where

$$\frac{\tau_{\omega 1}}{\tau_{\omega 2}} = \frac{|n_{c,1}(\omega_1)|}{|n_{c,1}(\omega_2)|} \left[\frac{1+\tan^2\phi(\omega_2)}{1+\tan^2\phi(\omega_1)} \right]^{1/2} \tag{A3}$$

for a constant modulation level G_1. Since $|n_{c,1}(\omega)| \sim |I(\omega)|$, changes in $\bar{N}$ can be directly derived from the phase shift, $\phi(\omega)$, *and* amplitude, $|I(\omega)|$. The validity of Eqs. (A2)–(A3) has been tested by comparing their results with numerical integrations of $N(E)$ curves after annealing and light soaking, and both methods have been found to yield the same results within 10% deviation.

Combining Eqs. (5) and (8) one finds

$$\int_{E_{Fn}}^{E_\omega} v\sigma N(E)dE = \frac{G_1}{|n_{c,1}(\omega)|[1+\tan^2\phi(\omega)]^{1/2}} - \frac{1}{t_{tr}} \ . \tag{A4}$$

For phase-shift measurements at low temperatures the deepest experimentally accessible demarcation energy $E_{\omega 0}$ is still above the deep-states peak (at $-100\,^\circ$C and 5 Hz: $E_{\omega 0} \approx 4.0$ eV), but with Eq. (A4) at least some estimate of changes in the deep-state density can be made. For instance, a drop of $|I(\omega_0)|$ upon light soaking implies, according to Eq. (4), either a shift of E_{Fn} towards midgap that must be due to an increase of deep states below E_{Fn} or an increase of $N(E)$ between E_{Fn} and $E_{\omega 0}$. In any case, changes in $|I(\omega)|$ always reflect a reverse change of $N(E)$ below E_ω.

The arguments above have been used to deduce changes in the deep-state density directly from measurements at low temperatures, and in the following some typical results are presented: When a sample is light soaked at $-100\,^\circ$C for 130 min, a drop of $|I(\omega_0)|$ by 12 dB compared to the annealed state is obtained. After reheating the sample to $60\,^\circ$C for 10 min and cooling the sample again to $-100\,^\circ$C, $|I(\omega_0)|$ has recovered to a large

degree being only 3 dB lower than in the annealed state. In contrast, when the sample is light soaked at 60 °C, a drop of $|I(\omega_0)|$ by 7.5 dB is obtained, but in this case no subsequent recovering has been detected even after extended storage at 60 °C. This clearly shows that creation of deep states is more efficient at lower temperatures but most of the created states anneal back when heating to environmental temperatures. The net effect—i.e., the remaining deep states at the measurement temperature (60 °C)—is the apparent activation energy of 30 meV for the creation efficiency.

When the change of deep-state density is derived from measurements at 60 °C using Eqs. (A2)–(A3), a drop of 10.5 dB (compared to 7.5 dB from above) and of 5.5 dB (compared to 3 dB) is obtained. Inspecting Eq. (A4), the lower values deduced from low-temperature measurements are probably due to a non-negligible $1/t_{tr}$ in Eq. (A4), but without knowledge of t_{tr} the qualitative behavior of deep-state density changes can at least be estimated.

When the samples were annealed under depletion bias, no changes in $|I(\omega_0)|$ at -100 °C were found, which means that the total density of deep states below $E_{\omega 0}$ does not change significantly although from measurements at 60 °C the peak at $E_c - 0.6$ eV has been found to increase. The only reasonable explanation is a corresponding decrease of deep states below E_F. This view is confirmed by the fact that E_F was found to shift towards E_c upon depletion bias annealing.

ACKNOWLEDGMENTS

This work has been supported by the Bundesministerium für Forschung und Technologie (Bonn, Germany) under BMFT Contracts No. 03E-8019-B and No. 03E-8327-B.

[1]P. G. LeComber and W. E. Spear, Philos. Mag. Lett. B **53**, L1 (1986).
[2]K. Tanaka and H. Okushi, J. Non-Cryst. Solids **66**, 205 (1984).
[3]J. Kočka, J. Non-Cryst. Solids **90**, 91 (1987).
[4]Y. Bar-Yam and J. D. Joannopoulos, Phys. Rev. Lett. **56**, 2203 (1986).
[5]Y. Bar-Yam, D. Adler, and J. D. Joannopoulos, Mater. Res. Soc. Symp. Proc. **95**, 3 (1987).
[6]G. Schumm, K. Nitsch, M. B. Schubert, and G. H. Bauer, Mater. Res. Soc. Symp. Proc. **118**, 543 (1988).
[7]G. Schumm, K. Nitsch, and G. H. Bauer, Philos. Mag. B **58**, 411 (1988).
[8]M. Stutzmann, W. B. Jackson, and C. C. Tsai, Phys. Rev. B **32**, 23 (1985).
[9]T. Tiedje, in *Semiconductors and Semimetals,* edited by F. I. Pankove (Academic, London, 1984), Vol. 21, p. C-207.
[10]H. Oheda, J. Appl. Phys. **52**, 6693 (1981).
[11]T. Tiedje and A. Rose, Solid State Commun. **37**, 49 (1980).
[12]J. D. Cohen and D. V. Lang, Phys. Rev. B **25**, 5321 (1982).
[13]D. V. Lang, J. D. Cohen, and J. P. Harbison, Phys. Rev. B **25**, 5285 (1982).
[14]A. Doghmane and W. E. Spear, Philos. Mag. B **53**, 463 (1986).
[15]R. A. Street, J. Zesch, and M. J. Thompson, Appl. Phys. Lett. **43**, 672 (1983).
[16]M. Stutzmann, W. B. Jackson, and C. C. Tsai, Phys. Rev. B **34**, 63 (1986).
[17]W.-J. Tzeng, H.-H. Tsai, and S.-C. Lee, J. Appl. Phys. **62**, 1856 (1987).
[18]W. E. Spear and P. G. LeComber, Philos. Mag. B **33**, 935 (1976).
[19]R. L. Weissfield and D. A. Anderson, Philos. Mag. B **44**, 83 (1981).
[20]N. B. Goodman and H. Fritzsche, Philos. Mag. B **42**, 149 (1980).
[21]P. Fenz, H. Müller, H. Overhoff, and P. Thomas, J. Phys. C **18**, 3191 (1985).
[22]R. A. Street and J. Kakalios, Philos. Mag. B **54**, L21 (1986).
[23]J. Kočka *et al.*, in *Proceedings of the 8th European Photovoltaic Solar Energy Conference and Exhibition, Florence, 1988,* edited by I. Solomon, B. Equer, and P. Helena (Kluwer Academic, Dordrecht, 1988), p. 724.
[24]F. Schauer and J. Kočka, Philos. Mag. Lett. B **52**, L25 (1985).
[25]H. Kakinuma, S. Nishikawa, and T. Watanabe, J. Non-Cryst. Solids **59-60**, 421 (1983).
[26]M. Stutzmann, Appl. Phys. Lett. **47**, 21 (1985).
[27]J. Kočka *et al.*, J. Non-Cryst. Solids **97-98**, 819 (1987).
[28]S. Guha, W. den Boer, S. C. Agarwal, and M. Hack, Appl. Phys. Lett. **47**, 860 (1985).
[29]S. R. Kurtz, Y. S. Tsuo, and R. Tsu, Appl. Phys. Lett. **49**, 951 (1986).
[30]Y. Okayasu *et al.*, in *Stability of Amorphous Silicon Alloy Materials and Devices (Palo Alto, 1987),* Proceedings of an International Conference on Stability of Amorphous Silicon Alloy Materials and Devices, AIP Conf. Proc. No. 157, edited by B. L. Stafford and E. Sabisky (AIP, New York, 1987).
[31]S. R. Elliot, Philos. Mag. B. **38**, 325 (1978).
[32]D. Adler, J. Phys. (Paris) Colloq. **42**, C4-3 (1981).
[33]D. Adler, Solar Cells, **9**, 133 (1983).
[34]M. Stutzmann and W. B. Jackson, Solid State Commun. **62**, 153 (1987).
[35]Z. E. Smith *et al.*, Phys. Rev. Lett. **57**, 2450 (1986).
[36]J. G. Simmons and G. W. Taylor, Phys. Rev. B **4**, 502 (1971).
[37]M. Stutzmann, W. B. Jackson, A.-J. Smith, and R. Thompson, Appl. Phys. Lett. **48**, 62 (1986).
[38]W. B. Jackson and J. Kakalios, Phys. Rev. B **37**, 1020 (1988).
[39]R. A. Street, C. C. Tsai, J. Kakalios, and W. B. Jackson, Philos. Mag. B **56**, 305 (1987).
[40]H. Yamagishi *et al.*, Appl. Phys. Lett. **47**, 860 (1985).
[41]D. Han and H. Fritzsche, J. Non-Cryst. Solids **59-60**, 397 (1983).
[42]Y. Nitta *et al.*, J. Non-Cryst. Solids **97-98**, 695 (1987).
[43]E. A. Niekisch, Ann. Phys. (Leipzig) **15**, 279 (1955).
[44]E. A. Niekisch, Ann. Phys. (Leipzig) **15**, 288 (1955).
[45]K. W. Boer and E. A. Niekisch, Phys. Status Solidi **1**, 275 (1961).
[46]E. A. Niekisch, Z. Phys. **161**, 38 (1961).